Contact-free measurement of surface tension on single droplet using machine learning and acoustic levitation

Citation for the original published paper (version of record):
Argyri, S., Evenäs, L., Bordes, R. (2023). Contact-free measurement of surface tension on single droplet using machine learning and
acoustic levitation. Journal of Colloid and Interface Science, 640: 637-646.
http://dx.doi.org/10.1016/j.jcis.2023.02.077

Journal of Colloid and Interface Science 640 (2023) 637–646

Contents lists available at ScienceDirect

Journal of Colloid and Interface Science

journal homepage: www.elsevier.com/locate/jcis

Contact-free measurement of surface tension on single droplet using machine learning and acoustic levitation

Smaragda-Maria Argyri, Lars Evenäs, Romain Bordes *

Department of Chemistry and Chemical Engineering, Chalmers University of Technology, Gothenburg 41296, Sweden

HIGHLIGHTS

- An acoustic levitator was used for contactless determination of surface tension.
- A dataset of over 50,000 photographs of levitated aqueous surfactant droplets was built.
- The droplet contours were processed through a neural network.
- Limitations of theoretical frameworks were surpassed by the machine learning approach.

GRAPHICAL ABSTRACT

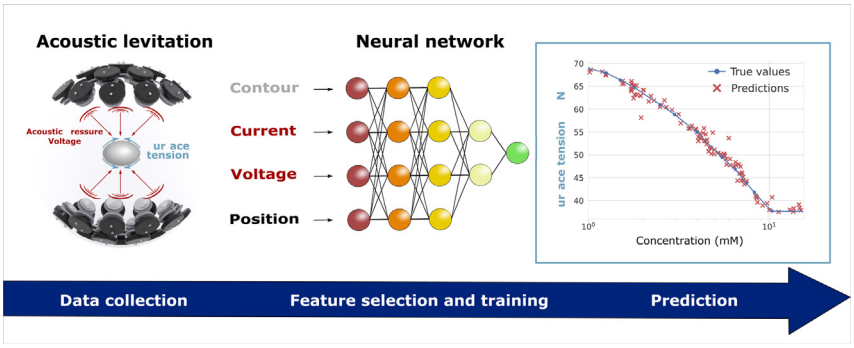

ARTICLE INFO

Article history:
Received 24 October 2022
Revised 2 February 2023
Accepted 14 February 2023
Available online 23 February 2023

2000 MSC:
0000
1111

Keywords:
Contact-free
Surface tension
Machine learning
Levitating
Droplet

ABSTRACT

Hypothesis: Acoustic levitation provides the possibility to deform levitated droplets in a controllable, and quantifiable manner, thus offering a means to measure the surface tension of a liquid droplet based on its deviation from sphericity. However, for new generation of multi-source and highly stable acoustic levitators, no model relates the acoustic pressure field to the deformation and surface tension. Utilizing a machine learning algorithm is expected to identify correlations between the experimental data without any set preconditions.

Experiments: A series of aqueous surfactant solutions with a large range of surface tensions were prepared, and evaporated under levitation, while the acoustic pressure was varied. A dataset of over 50,000 images was used for the training and evaluation of the machine learning algorithm. Prior to that, the machine learning approach was validated on in silico data that also included artificial noise.

Findings: We achieved high accuracy in predicting the surface tension of single standing droplets (±0.88 mN/m), and we surpassed certain physical conditions related to the size, and shape of the suspended samples that simpler theoretical models are subject to.

1. Introduction

Most commonly the measurement of surface tension involves the use of a solid object (*e.g.*, needle, Du Noüy ring, Wilhelmy plate *etc.*), which poses the major risk of contamination, or surface induced error. Acoustic levitation constitutes an appealing method to levitate, and manipulate small volume droplets of liquids, thus minimizing such shortcomings. The major advantage of acoustic levitation over other levitation techniques (*e.g.*, magnetic levitation, optical tweezers, *etc.*) is that acoustic waves interact with matter regardless of properties like magnetism, dielectricity *etc.*.

* Corresponding author.
E-mail address: bordes@chalmers.se (R. Bordes).

https://doi.org/10.1016/j.jcis.2023.02.077
0021-9797/

In the case of a liquid suspended in an acoustic levitator, the droplet will deviate from a spherical shape (*i.e.*, minimum surface area governed by surface tension), to an ellipsoid (Fig. 1a), due to the applied acoustic pressure. In Fig. 1b, the simulation of the acoustic pressure field of the acoustic levitator used in this study is depicted. The areas of low pressure (*i.e.*, acoustic nodes) act as physical traps since the surrounding high pressure constrains the levitated object around the center of the node (z = 0 mm, Fig. 1b). The main forces governing the droplet deformation are the surface tension, acoustic radiation force, and gravitational force (Fig. 1c). Surface tension, which tends to minimize the surface free energy of the droplet by reducing its surface area, will oppose deformation. On the contrary, the acoustic radiation force on the surface of the droplet will promote it. The weight of the droplet will affect its vertical position with respect to the acoustic node ($z < 0$ mm, Fig. 1b) [1]. Hence, for heavier droplets the surface acoustic pressure (SAP, Fig. 1c) will be higher, consequently the shape will deviate more from sphericity. Furthermore, the gravitational force impacts the deformation to a larger extent, when the radius of the droplet is larger than the capillary length, λ_c. In that case, the gravitational force will be higher than the Laplace pressure, and as a result, the droplet will be flattened at the top, due to its own weight.

As shown in Fig. 1d, for fixed voltage, and surface tension, the droplet tends to be more spherical for smaller volumes. This is attributed to the acoustic radiation force applied on the surface of the droplet. The heavier the droplet, the lower the vertical position, z of the droplet will be, thus the acoustic radiation force will induce a greater deformation. On the contrary, a smaller droplet will be positioned closer to the center of the node. Therefore, the acoustic pressure applied on the surface of the droplet will be lower, thus the droplet shape will be closer to spherical. When

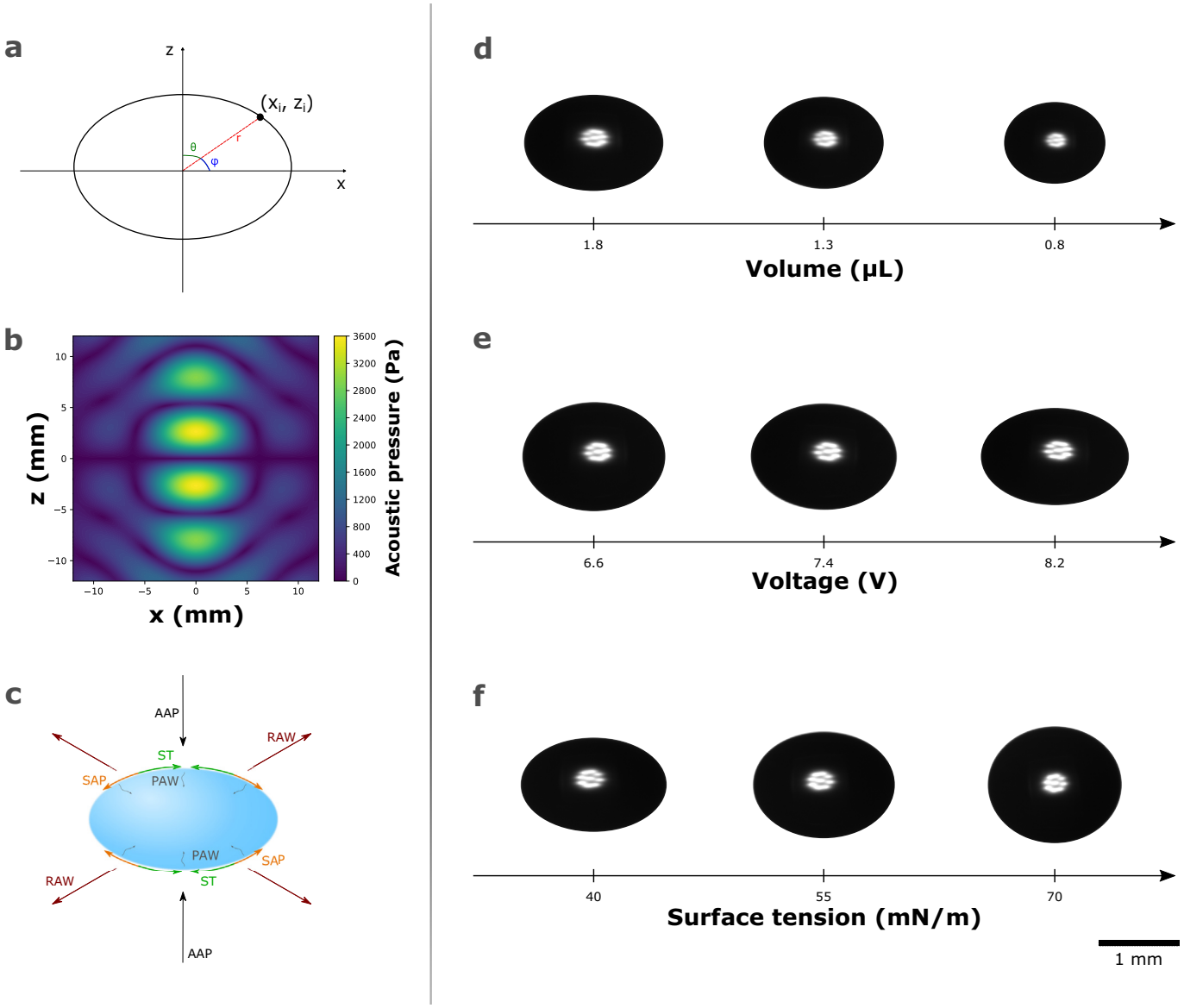

Fig. 1. (a) Coordinate system, where r polar coordinate radius, ϕ polar coordinate angle, and θ azimuth angle. (b) Simulation of the acoustic pressure field generated by the acoustic levitator used in this study. (c) Illustration with the forces applied on the levitated droplet: AAP: applied acoustic pressure, RAW: reflected acoustic waves, SAP: surface acoustic pressure, PAW: penetrating acoustic waves ST: surface tension. (d) Photographs of levitated droplets with constant surface tension (29 mN/m), and voltage (9.0 V) showing the correlation between the droplet shape, and the volume. (e) Photographs of levitated droplets with constant volume (2.1 μL), and surface tension (48 mN/m) showing the correlation between the droplet shape, and the voltage. (f) Photographs of levitated droplets with constant volume (2.0 μL), and voltage (7.0 V) showing the correlation between the droplet shape, and the surface tension.

the volume and surface tension are constant, the deviation from sphericity will be greater as the applied acoustic pressure increases (Fig. 1e, where the voltage is used as a measure of the acoustic pressure intensity). In contrast, a droplet with lower surface tension requires less acoustic radiation force to be deformed, for the same volume, and voltage, as shown in Fig. 1f. In all cases described above, the radius of the droplets is below the capillary length.

From the examples above, it is clear that the description of the deformation relies on a simple principle (*i.e.*, balance of applied forces), yet a major difficulty lies in the accurate description of the surface acoustic pressure of the self-standing droplet. The acoustic pressure field generated by acoustic levitators can be described in a relatively straightforward manner, assuming that each ultrasonic transducer acts as a point source. However, the acoustic pressure field is affected by the levitated object, due to reflected acoustic waves from the surface of the droplet, while the acoustic waves that are not reflected will be absorbed by the droplet. Another complication is that the surface acoustic pressure changes with droplet volume, as described above.

In the case of the Langevin horn (*i.e.*, a simple single source, uniaxial levitator), Trinh and Hsu, [2] experimentally evaluated the theory that correlates the shape of the droplet, the volume, and the acoustic pressure, with the surface tension. However, a significant amount of constraints have to be accounted for, to simplify the equation systems. As a result, the derived equation is valid for spherical or nearly spherical droplets with a volume less than 2.5 μL. These conditions limit the experimental conditions, and choice of studies, significantly. Later on, Tian *et al.*, [3] developed an analytical solution that could estimate the shape of an acoustically levitated droplet, and its position within the acoustic pressure field for larger droplets. In a following publication Tian *et al.*, [4] applied the analytical approach to determine the surface tension of acoustically levitated samples. It was estimated that the sensitivity of the method was ±2 mN/m for surface tension values lower than 50 mN/m. It was stated that the reason the sensitivity was low compared to other techniques (typical statistical error: $\pm 0.1 - 0.5$ mN/m [5]), due to low stability of such type of acoustic levitator. Langevin horns are often reported as difficult to operate [6], owing to extremely low lateral forces, which may cause the suspended droplet to escape the acoustic node sideways (Fig. S1b, Supporting Information).

Recently, Marzo et al. [7] designed a new generation of acoustic levitators that uses multiple ultrasound transducers operating at low voltage. The transducers are positioned in a spherical configuration, which provides enhanced control, and unprecedented stability of the levitated droplet, due to higher lateral forces (Fig. S2b, Supporting Information). This type of setup delivers higher acoustic pressure close to the acoustic node (Fig. 1b). Therefore, the shape of the droplets can be compressed more easily in comparison to the Langevin horn, thus limiting the use of the existing theoretical models for the determination of surface tension.

To circumvent this issue we took advantage of the high stability of multi-source acoustic levitators and employed a data-driven approach through a machine learning algorithm that established correlations between the surface tension, and deformation of the droplets, depending on the volume, position in space, voltage, and current. This approach presents several advantages over a mathematical estimation of the acoustic pressure field, that would then be used to correlate surface tension and deformation. Firstly, the required inputs for the machine learning algorithm can be directly, and easily accessed from the experimental setup, in the form of voltage and current consumption. For instance, the acoustic pressure, which is usually difficult to measure accurately through a microphone, can be replaced by the applied voltage. The second advantage is that the neural network intrinsically accounts for the experimental errors, and provides a resilient system for which the accuracy can be higher than that of traditional models. Lastly, special cases (*e.g.*, big droplet, large deformations, very low surface tension *etc.*) that would normally require a specialized theoretical framework, could be accounted for by the same machine learning algorithm, provided that these extreme cases were represented in the training dataset.

In this study, we built a more compact multi-source acoustic levitator, compared to TinyLev et al. [7], which led to enhanced stability of the levitated sample. The setup (Fig. S3, Supporting Information) enabled the acquisition of a large experimental dataset, that consisted of over 50,000 photographs of levitated aqueous surfactant droplets. The high data availability enabled the application of a machine learning-based approach. The machine learning aspect of the study was divided into two parts. Firstly, we investigated the validity of a data-driven approach using a simplified mathematical model for Langevin horns. This model allowed the generation of contours based on initial conditions (*i.e.*, acoustic pressure, volume, surface tension) which constituted the in silico dataset. This dataset was used to construct the architecture of a supervised neural network (NN), and to evaluate the effect of artificially generated noise on the accuracy of the predictions. The neural network was then trained with experimental data, for which the acoustic pressure parameter was substituted by the driving voltage of the levitator, the current consumption, and the position of the droplet along the z-axis. With this methodology, we demonstrate that deformation of acoustically levitated data can be processed with a data-driven approach toward the prediction of meaningful measurements, while avoiding the need of developing complex models.

2. Experimental section

2.1. Chemicals

Sodium dodecylsulfate (SDS) was provided by Merck, cetyltrimethylammonium bromide (CTAB), and Triton X-100 were purchased from Sigma–Aldrich Sweden AB.

2.2. Surfactant solutions preparation

Series of aqueous solutions of SDS (0.01 – 100 mM), CTAB (0.001 – 96 mM), and Triton X-100 (0.0001 – 10 mM) were prepared in milli-Q water, at 23 °C. The solutions were stored at room temperature for up to 5 days. The measurements were acquired within a maximum of 3 days after the solution was prepared.

2.3. Surface tension measurements

The surface tension of the surfactant solutions was measured with the pendant drop method, using an Attension Theta optical tensiometer, by Biolin Scientific, Finland. A minimum of 10 droplets were formed with a 0.718 mm needle, and let for equilibrating for about one minute before starting the measurements that would last for 3 min, following the practice described in [8]. An average of the equilibrated values was then taken. Longer recording times were not considered as the effect of evaporation was noticeable. A black and white digital camera is used to record images of droplets, and the surface tension is determined by fitting the Young–Laplace equation on the contour of the droplet.

2.4. Acoustic levitation

The acoustic levitator was built based on the TinyLev levitator presented by Marzo et al. [7]. The scaffold of the device was 3D

printed with polylactic acid (PLA), and it consists of 36 ultrasonic transducers in total, 18 at the top, and 18 at the bottom. Each transducer operates at a frequency of 40 kHz. The driving voltage ranged between 6.5 to 11 V. Description of the setup is found on https://github.com/sargyri/Drop_Lev.

2.5. Simulation of acoustic pressure field

The simulations of the acoustic pressure fields were generated through the Python library *Levitate* [9]. Each transducer is considered a point source, with directivity of a circular ring, and the acoustic pressure is calculated as a superposition of the single sources. The acoustic pressure of a single transducer is given by [10]:

$$p_j = \frac{e^{ikr_j}}{r} J_0(kr_j \sin(\theta_j)) \quad (1)$$

where r_j is the distance between a transducer j and the levitation point, θ_j is the angle between a transducer j and the z-axis, and J_0 is the Bessel function of the first kind of order 0.

The Python code used for the following simulations can be found on https://github.com/sargyri/Drop_Lev.

2.6. Generating in silico data

Trinh and Hsu, [2] utilized a Langevin horn to study the deformation of liquid droplets in an acoustic pressure field. They established the mathematical expression below, to describe the equilibrium shapes of acoustically levitated droplets based on the theory presented by Marston et al. [11,12]:

$$r(\theta) = R + x(\theta) \quad (2)$$

where θ is the azimuth angle (Eq. (S2), Supporting Information), and R the equivalent spherical radius of the droplet. Parameter $x(\theta)$ describes the deviation from sphericity and is expressed as

$$x(\theta) = -\frac{3}{64\sigma}(3\cos^2(\theta) - 1)R^2 P_s^2 \beta_0 \left(1 + \frac{7}{5}(kR)^2\right) \quad (3)$$

where σ is the surface tension, and β_0, and k the compressibility and wavenumber of the host medium (*i.e.*, air), respectively.

This equation was derived by applying the Gor'kov potential to describe the acoustic radiation force, which is valid only for spherical objects with a radius below 1/10 of the operating wavelength, λ_o of the device ($f = 40$ kHz for the acoustic levitator used for this study):

$$\lambda_o = \frac{u}{f} \quad (4)$$

where, u is the speed of the speed in air and f is the operating frequency.

Another condition that should be fulfilled is that the gravitational force must not exceed the Laplace pressure. For this condition to be true, the droplet radius needs to be lower than the capillary length (λ_c), which is defined as

$$\lambda_c = \sqrt{\frac{\gamma}{\rho * g}} \quad (5)$$

where, γ is the surface tension, ρ the density, and g the gravity acceleration.

In total, 70,000 contours were generated from Eqs. (2) and (3), while the variation range of the input parameters is shown in Table 1.

Each contour was described by 900 data points in terms of the polar radius and the azimuth angle. This number of points corresponds to the average experimental contour points library OpenCV provides when it extracts the contour from the image. To ensure that the coordinates are evenly distributed, and describe the contour well, the 900 contour points were interpolated, then the polar coordinate, ϕ was set constant, and the radius, r was determined through the interpolation fit.

Table 1
Range of input parameters for the generation of in silico drop contours.

Parameter	Min value	Max value
Volume (μL)	0.50	2.50
Surface tension (mN/m)	30.00	72.00
Acoustic pressure (Pa)	1,500	4,000

The two conditions related to the wavelength and capillary length were applied to the in silico data to eliminate the contours that did not apply to these conditions. An additional threshold was set on the aspect ratio to ensure that the generated contours were physically valid. As shown in Fig. S4d (Supporting Information), certain contours appear to have a negative curvature, which does not correspond to an equilibrium droplet shape, since in that case, the droplet would have burst. Even after the first two conditions were applied, some contours had a negative curvature. For that reason, only the contours with an aspect ratio between 0.66–1 were included in the dataset. Representative examples of the applied thresholds can be found in Fig. S5, Supporting Information.

The input features used for the training of the neural network with in silico data were the 175 radii evenly distributed around the contour, and the acoustic pressure. The surface tension was considered the target feature (*i.e.*, the value that the neural network was trained to predict).

2.7. Addition of artificial noise on in silico data

Noise was added on the in silico contours, to assess the effect of the potential experimental error on the ability of the neural network to successfully derive correct surface tension predictions. From our experience, the main source of noise originates from the degree of instability the levitator exhibits while the setup was steady. The more unstable a levitator is, the more the droplet will move in the air. When the movement takes place in the xz plane (view Fig. 1d) - horizontally, and vertically - it can induce blurriness in the images. Subsequently, if the droplet moves in the y plane (*i.e.*, forwards, and backward) it can appear larger when it is closer to the camera, or smaller (*i.e.*, lower volume) when the droplet is further away from the camera. Additionally, we assumed that the contour was defined by ±0.5 pixel.

To replicate the experimental noise, artificial noise was added to the polar radius to ensure equivalent error distribution along the contour. The degree of noise is defined in pixels and converted into millimeters. The contour disturbance added resulted from the multiplication of the degree of noise with a random number between 0 and 1 (view Eq. (6)).

$$\begin{aligned} \text{disturbance} &= \text{degree of noise} * \text{calibration factor} \\ &\quad * \text{random number} \\ &\in [0, 1] \end{aligned} \quad (6)$$

The lowest limit for the degree of noise was set at 0.5 pixels. The upper limit was chosen to be 5 pixels, which produced a realistic maximum experimental noise, caused by blurred droplet boundaries due to levitation instabilities. The contour disturbance was applied on all contours. The noisy dataset was split into 80% training data and 20% test data with the same random state number used in the in silico dataset without noise. The random state number ensures that the splitting will contain the same random contours every time you repeat it. Then the model was trained with the noisy training dataset and its accuracy was evaluated through

the MAE value on the test dataset. The training and evaluation were repeated 6 times and the standard deviation was calculated.

As mentioned above, the choice of radii was performed by defining an array of 175 polar angles, ϕ, equally distributed around the contour and interpolating around the contour. If the droplet is slightly tilted in the xz plane, the radii will not be at the exact same positions, which leads to data inconsistencies. This can occur if either the camera or the levitator is perfectly aligned vertically. The following equations were applied for determining the tilted x and y coordinates of the contours:

$$x_{\text{tilt}} = \cos(\text{tilt\_angle}) * x - \sin(\text{tilt\_angle}) * y \quad (7)$$

and,

$$y_{\text{tilt}} = \sin(\text{tilt\_angle}) * x + \cos(\text{tilt\_angle}) * y \quad (8)$$

where x_{tilt} and y_{tilt} are the tilted x and y coordinates, *tilt_angle* the tilting angle around the y-axis, while x and y are the Cartesian coordinates describing the initial contour Cartesian coordinates.

The contours in the in silico dataset were randomly tilted along the y-axis within an angle range from 0 to the maximum tilt angle (*e.g.*, from 0 to ±25°). The dataset was split into 80% training and 20% test data, with the same random splitting applied on the in silico dataset without noise, as described above. The training of the machine learning algorithm was repeated 6 times, and the MAE was used as the evaluation parameter.

In all cases, the MAE of each noisy dataset was compared to the MAE produced by the function *Dummy Regressor* from the Sklearn library. This regressor calculates the average value of the target feature (*i.e.*, surface tension) in the training dataset and returns that value as a prediction for all cases in the test dataset. It describes the condition at which the neural network is not gaining any insight from the training. Therefore, it sets an upper-performance boundary of MAE the neural network may return for a specific dataset.

2.8. Experimental data acquisition

A digital camera (acA1440-220um, Basler, Germany) was utilized to capture images of the droplets over time. The contours of the droplets were extracted using python and *via* the OpenCV library. The Canny edge detection algorithm [13] along with the findContour function [14] were used to identify the droplet edges. The calibration of the camera (mm/pixel) took place with the help of a disposable needle with a known diameter (0.83 mm). The image resolution (calibration factor) corresponded to 3 μm/pixel, for the chosen setup. Each levitating droplet was left evaporating over a period of 30 min, and images were captured at 1 fps. The voltage was varied continuously with a rate of 0.01 V/s. The volume of the droplet was calculated according to the disk method (Eq. (S1), Supporting Information). Since the volume and the initial concentration of the droplet were known, we used the adsorption isotherms (Fig. S8, Supporting Information) to back-calculate the surface tension of the droplet at any point in time.

It was observed experimentally, through the OpenCV library, that a tilting angle of maximum 5–6° may occur. For that reason, all contours were corrected for tilting, through Eqs. (7) and (8). Another source of data irregularities that may arise is related to the position of the center of the droplet. The Python library OpenCV sets as point (0,0) the upper left corner of the image. Consequently, the coordinates, and thus the position of the center will depend on the relevant position of the experimental equipment. For that reason, the center of each droplet was offset and centered around the point (0,0). In the final csv file with the data, each row corresponds to one frame, and each column to one characteristic of the depicted droplet (*e.g.*, coordinates, volume, voltage, *etc.*).

2.9. Machine learning algorithm

The ability of the neural network to predict surface tension from the droplet's characteristics was initially evaluated on in silico data without noise. Then, noise was added to the in silico data, to test the robustness of the algorithm. Finally, the neural network was used on the experimental data of acoustically levitated droplets of surfactant solutions. The input features in the case of in silico data were 175 polar radii, r that were equally distributed around the contour and the acoustic pressure that was used as input in Eq. (3). For the experimental data, the input features were again 175 radii, but the acoustic pressure was substituted by the vertical position, voltage, and current. In both cases, the output of the neural network (*i.e.*, target feature) was the surface tension.

The following procedure was applied on both in silico and experimental datasets, thus generalized terms are used. Initially, the dataset was split into training (80% of the total data), and test dataset (20% of the total data). The training of the neural network (Table 2) was performed on 80% of the training dataset, and the rest 20% was used for validation. The neural network has access to both the input features in addition to the target feature of the training dataset. The training thus enables the creation of correlations that provide a prediction of surface tension. The ability to predict surface tension accurately was then evaluated through the test dataset, where the neural network has access only to the input features.

The training dataset was normalized to feature values between 0 and 1. This was performed by finding the maximum value of each feature (*i.e.*, column) in the training dataset, and then dividing the whole column by that value. The values in the test dataset were transformed based on the maximum values in the training dataset. If the test dataset was utilized to transform the range of the data, access to the surface tension values would be required, which will not be the case when the algorithm needs to be applied on experimental data. This means that the data range of the test dataset may be below 0 and above 1, depending on the maximum values of the training dataset, which shows the applicability of a machine learning algorithm on data outside the training range.

The architecture of the neural network can be seen in Table 2. The neural network consists of 8 fully connected layers. The number of neurons from the top layer to the bottom is 50, 40, 30, 20, 15, 10, 5, and 1 neuron(s). The "swish", and "softplus" activation functions, and the "Adam" optimizer used were from the TensorFlow library.

Subsequently, the training and evaluation of the machine learning model were performed on the training, and test datasets, respectively. The mean squared error (MSE) was used as the minimization parameter (*i.e.*, the model will store the weights, and biased of each layer that leads to the minimum MSE). The model that led to the minimum MSE was saved, and tested on new data, to evaluate the ability of the model to predict on new data (*i.e.*,

Table 2
Summary of the neural network model developed for the prediction of surface tension. The output shape defines the number of neurons present in each layer, and the number of parameters is shown in the last column. The total number of trainable parameters is 13,376.

Layer (type)	Output Shape	No. Parameters
dense 0 (Dense)	(None, 50)	8,950
dense 1 (Dense)	(None, 40)	2,040
dense 2 (Dense)	(None, 30)	1,230
dense 3 (Dense)	(None, 20)	620
dense 4 (Dense)	(None, 15)	315
dense 5 (Dense)	(None, 10)	160
dense 6 (Dense)	(None, 5)	55
dense 7 (Dense)	(None, 1)	6

generalization). An open source framework containing the machine learning algorithms and the data is available on https://github.com/sargyri/Drop_Lev.

2.10. Feature importance

The contribution of each feature to the prediction error of the neural network was investigated through a permutation feature importance algorithm, introduced by Fisher, Rudin, and Dominici (2018) [15].

The employed algorithm is described as follows.

- The MAE of the neural network, when no feature is permuted, is determined by training the model and predicting on the test dataset.
- One feature is permuted at a time, by shuffling the rows of the column. The MAE is determined by using the trained model and predicting on the test dataset.
- When all features are permuted, and the corresponding MAE are saved, we compare the MAE before, and after permutation. The feature importance is defined as $FI = MAE_{after} - MAE_{before}$.
- The procedure is repeated 3 times for statistical purposes.

This algorithm allows the investigation of the influence each feature has on the machine learning predictions. It should be pointed out that this method is not used to add interpretability to the neural network, but to evaluate the choice of features used in the training, and whether this choice has a physical meaning. The higher the difference between the MAE before, and after permutation, the greater the influence of the feature on the predictions. For more information on machine learning interpretability the reader may refer to the book by C. Molnar [16].

3. Results and Discussion

3.1. Validation of machine learning approach on in silico data

To examine the ability of the machine learning algorithm to determine the surface tension, we used Eqs. (2) and (3) to generate 70,000 in silico contours by using as inputs in the equation the volume, acoustic pressure, and surface tension. In Fig. S4a-c (Supporting Information), is shown the volume, acoustic pressure, and surface tension distributions for the 70,000 generated contours, while Fig. S4d (Supporting Information) shows the overlapped generated contours. Physical restrictions were applied so that the contours had physical validity (*i.e.*, no negative curvature, see Fig. S4d, Supporting Information). The restrictions eliminated 19,453 contours, which left 51,956 contours that were physically meaningful. The new data distributions and contours are shown in Fig. 2a-d.

The range of volume, acoustic pressure, and surface tension were chosen based on two criteria: to simulate realistic experimental conditions, and to eliminate the least amount of contours possible. Specifically, the volume range was between 0.5 and 2.5 μL. The upper volume limit was set so that the majority of the contours will be in accordance with the shape restrictions the Gor'Kov theory sets, while the minimum limit was chosen based on experimental observations. The acoustic pressure range was between 1.5–4 kPa and it was chosen in accordance with the pressure range reported by Trinh and Hsu, [2]. The surface tension was selected to be in the range of 30 to 72 mN/m as the typical surface tension range of aqueous surfactant solutions.

In Table 2, the architecture of the chosen neural network is shown. The features that were input in the neural network were 175 radii describing each contour, and the acoustic pressure for the respective contour, while the surface tension was the output (*i.e.*, target feature). The dataset was split into training (80% of the dataset), and test data (20% of the dataset). Before importing the training data in the neural network, all data were preprocessed by transforming the features column-wise in the range between 0 and 1, based on the range values of the training dataset. In Fig. S6a-b (Supporting Information), the evolution of the mean absolute error (MAE), and the mean squared error (MSE) during training are shown. It can be observed that the traces of the training, and validation errors, are in good agreement for both error parameters, which indicates that the neural network fits the data well without overtraining. In Fig. 2e, the predictions are compared with the surface tension values from the test dataset that were input in Eq. (2). Each scattered point corresponds to one in silico contour, while the color bar expresses the density of points. It is observed that all points are on the diagonal, which represents the ideal case where the real values are equal to the predicted ones. The average mean absolute error (MAE) was equal to 0.06 mN/m. From the error distribution of the test dataset is shown in Fig. 2f, it was found that 100% of the predictions are in the range of ±0.5 mN/m, which corresponds to the statistical error of common surface tension measurement techniques.

3.2. Validation of machine learning approach on in silico data with artificial error

During the experiments, two main types of error may arise: blurriness around the contour due to the movement of the droplet, and tilted contours in case the camera, and the acoustic levitator are not well aligned. The sensitivity of the camera lies in the range of ±0.5 pixel. However, we have experimentally observed that for our setup, contour blurriness may lie in the range of ±0–3 pixels. To investigate the effect of blurriness on the ability of the machine learning algorithm to predict the surface tension, distortion in the range of ±0–5 pixel was added on all contours to simulate the most extreme case. The same neural network model (Table 2) was evaluated on noisy data, while as in the case of in silico data without noise, the input features were 175 radii describing each contour, and the acoustic pressure.

The training and evaluation of the machine learning algorithm were performed for each case of contour distortions (Fig. 3a), and the MAE was used as a tool to assess the performance of the model. Fig. 3b shows the relation between the MAE, and the distortion of the contours. It is observed that the MAE increases as the contour distortion increases. The error increase is expected since high contour distortion can potentially alter the features that the neural network recognizes, and derives the predictions from. Fig. 3c shows that the error distribution becomes wider as the contour distortion increases. The error range increases incrementally from ±0.5 mN/m, when no noise is added, to ±3 mN/m, when 5 pixels of noise are added.

The highest MAE value was compared with the result of the *Dummy Regressor* function. Through this function, all the predictions are equal to the mean surface tension value of the training dataset. Hence, this provides the highest MAE that we would expect in the case where the neural network was predicting randomly. The MAE calculated by the *Dummy Regressor* was 10.1 mN/m (Fig. S7, Supporting Information). Consequently, even at the highest introduced degree of noise, we have not reached the upper MAE limit which means that even though the error increased, the neural network does not predict randomly, but in fact learns from the training dataset, even if more errors are made.

Each contour was described by keeping the polar angle, ϕ constant, and interpolating to find the radius, r at that angle. In case a droplet is tilted, the interpolated radius, r will not correspond to the correct polar angle ϕ. Experimentally the tilt angles range from 0 to 5°. To simulate this case, the contours were randomly tilted

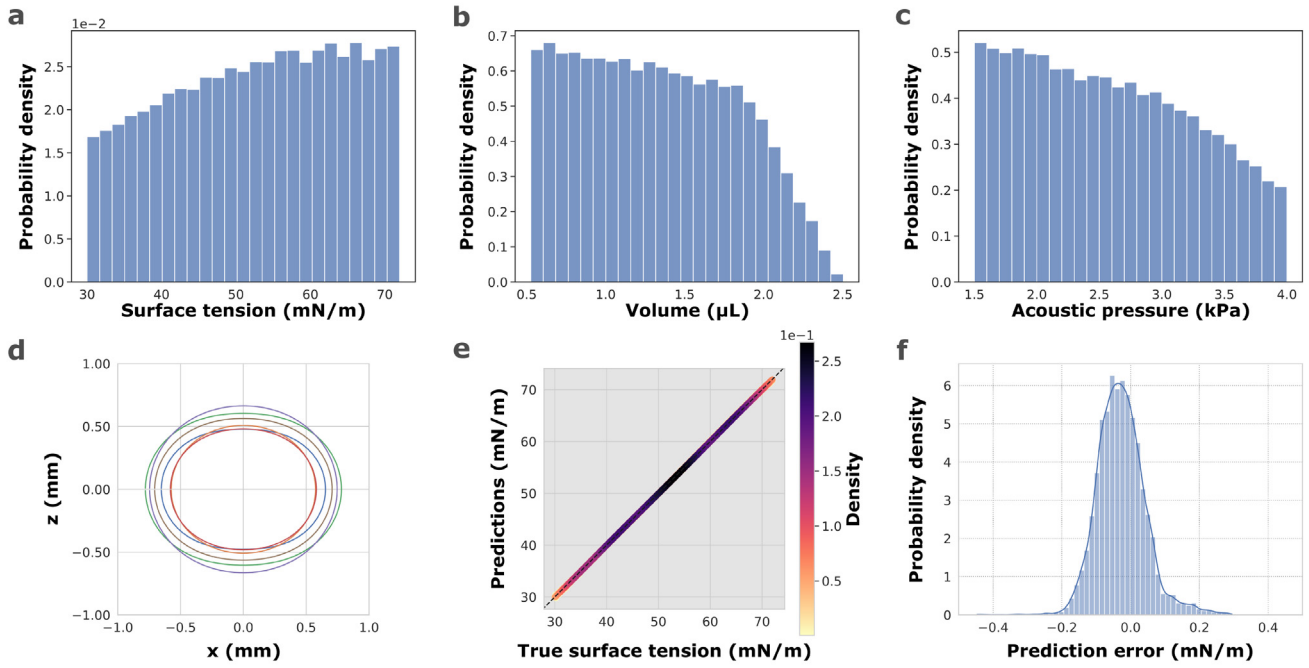

Fig. 2. In-silico data distribution of (a) volume, (b) acoustic pressure, and (c) surface tension of 51,956 contours after restrictions were applied. (d) Examples of contours generated based on the given (a-c) parameters. (e) Comparison between the true surface tension values (*i.e.*, used as input in Eqs. (2) and (3)), and the predicted values (*i.e.*, output of neural network). The darker the area, the more densely packed it is with scattered points. (f) Error distribution of the machine learning pred.ictions in mN/m.

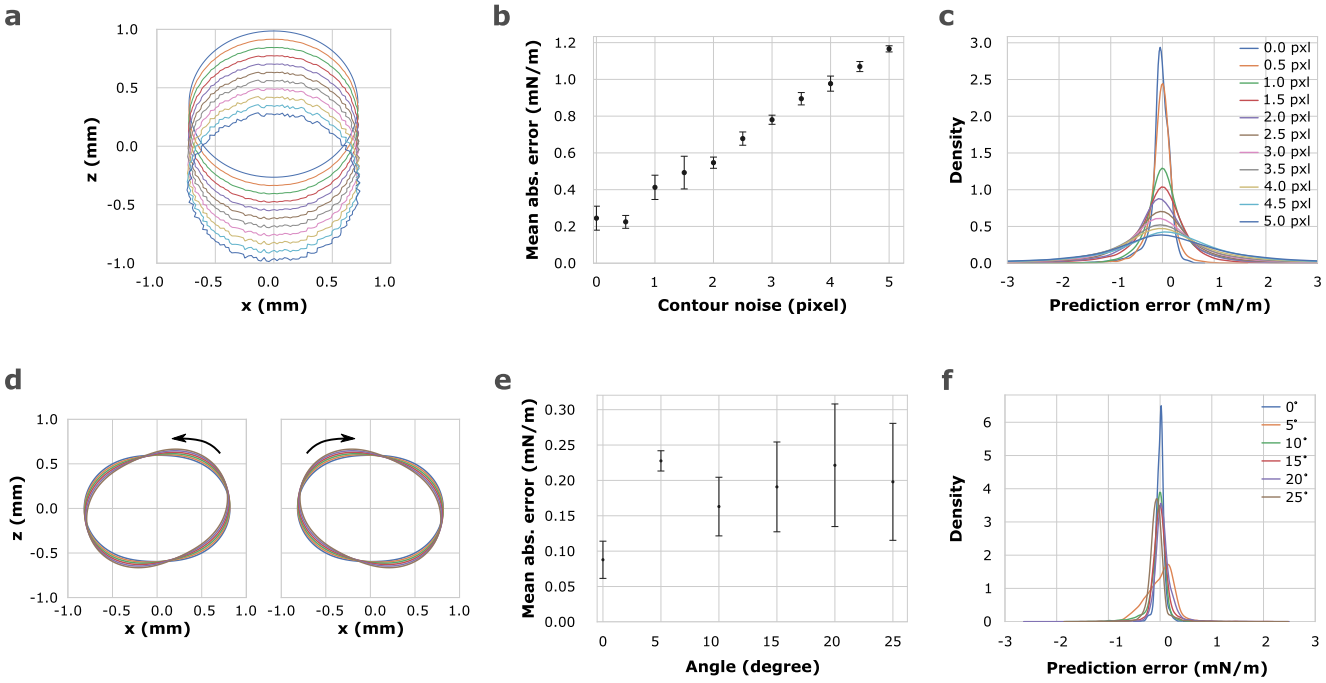

Fig. 3. (a) Contours were increasingly distorted to simulate experimental noise that can arise from the instability of the acoustic levitator. The contours are shifted vertically for illustration purposes. (b) The mean absolute error (MAE) is plotted as a function of the degree of contour distortion in pixels. (c) The error distortion of the predictions as the distortion increases. The predictions were repeated 6 times, and an average was calculated. (d) The contours were randomly tilted with an increasingly larger tilting angle. (e) The mean absolute error (MAE) is plotted as a function of the maximum tilting angle. (f) The error distribution of the machine learning predictions is plotted for each tilting angle. The predictions were repeated 6 times, and an average was calculated.

(Fig. 3d) within an angle range from 0° to the maximum tilt angle (*e.g.*, from 0 to ±25°). The training and prediction of the machine learning algorithm were repeated 6 times, and the MAE was evaluated. Fig. 3e shows the MAE with respect to the maximum tilting angle. It is observed that the error increases when tilting is induced. However, no clear correlation between the tilt, and the error is distinguished. Furthermore, the MAE is not as large as the one caused due to contour distortion. This is most likely

attributed to the spherical shape the majority of the in silico contours have after the physical restrictions are applied. As a result, little or no difference is caused on the interpolated radius, *r*, due to tilting.

3.3. Machine learning approach on experimental data

A series of aqueous surfactant solutions at different starting concentrations were prepared. Three different surfactants were chosen: sodium dodecyl sulfate (SDS, anionic), cetyltrimethylammonium bromide (CTAB, cationic), and Triton X-100 (non-ionic). The surface tension of the solutions was determined through the pendant drop method and plotted as isotherms (Fig. S8, Supporting Information). This allowed the calculation of the surface tension at any concentration when the starting concentration and the volume of the droplet at any point in time are known. The experimental data were collected by capturing images of the levitated droplet over a period of 30 min, with a frame rate of 1 frame per second. For each solution, the measurements were repeated 3 times. A total of 322,145 contours were detected. From those, 58,368 contours were chosen for the training.

The choice of data was made with the intent to have a relatively uniform surface tension distribution and to cover the adsorption isotherm of each surfactant equally well. That way we could avoid introducing a form of bias in the algorithm, and we could examine the level of accuracy of the predictions throughout the isotherm, respectively. The distributions of surface tension, volume, and voltage of the experimental data are shown in Fig. 4a-c. In Fig. 4d, representative examples of droplet contour are shown.

In accordance with the previous results, the dataset was preprocessed by correcting for the tilting, and the vertical position (see Methods) to eliminate this form of experimental error. Following, the dataset was split in the same way as for the in silico generated data: into 80% training (46,694 instances), and 20% testing (11,674 instances). Furthermore, the values of the features were processed as previously.

The same neural network architecture used for the surface tension prediction on in silico data was applied (Table 2). In this case, the input features were: 175 radii describing the droplet contour, the voltage, the current, and the position of the droplet along the z-axis. By comparing the training, and validation curves (Fig. S6c-d, c-d, Supporting Information), no overtraining was observed, since the MAE, and MSE curves overlap.

From Fig. 4e, it is observed that the majority of the predictions agree with the true surface tension values that were measured through the pendant drop method. Furthermore, it is observed that the neural network appears to perform very well within the lower surface tension values (ST $<$ 40 mN/m). This is due to the fact that in that range the droplets tend to be smaller, and more deformed. In Fig. 4f, the error distribution is shown, from which we calculated that the network shows 70% confidence that the surface tension error will be in the range of $\pm$1 mN/m, while the average MAE was found to be 0.88 mN/m.

In Fig. 5a-c, we observe that the predictions from the test dataset are in good agreement with the pendant drop measurements throughout the adsorption isotherms of all 3 surfactants used for the training, while very few outliers are observed.

Moreover, a feature importance analysis through permutation was performed in order to gain insight into how the machine learning algorithm weighs each feature, towards making a prediction. This allows a qualitative investigation of how logical the decisions are, and how well they reflect the physical reality. In Fig. 6a, the mean absolute error increase when a feature has been permuted is shown. It is observed that cumulatively the radius has the greatest effect on the predictions, followed by the voltage, current, and vertical position. In Fig. 6b, the importance of the coordinates is color coded, with the dark purple signifying higher importance and the light yellow the lowest. Hence, it is seen that the extreme contour points (*i.e.*, top, bottom, left, right) have the

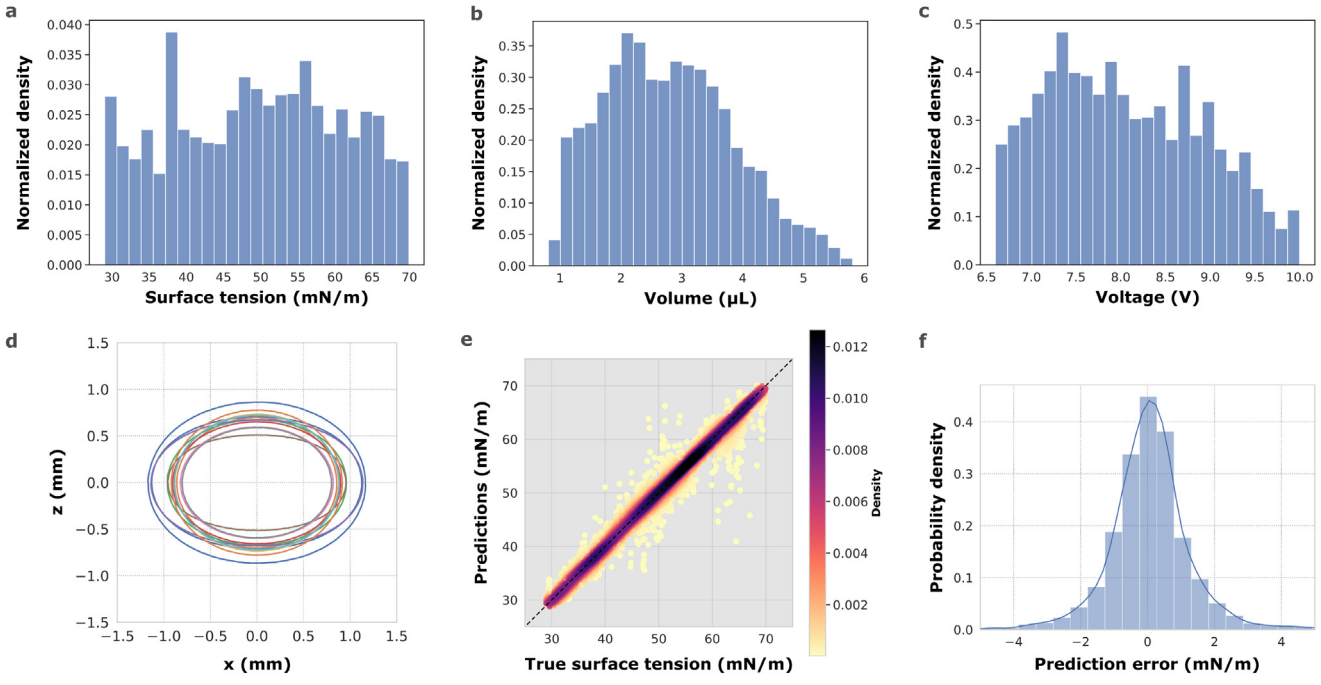

Fig. 4. Data distribution of experimental data (a) surface tension, (b) volume, (c) voltage of 58,368 contours from various SDS, CTAB, and Triton X-100 solutions. (d) Representative contours. (e) Comparison between the true values, and the predicted values of the test dataset (11,674 instances). (f) Error distribution of the machine learning prediction on the test dataset (11,674 instances), in mN/m.

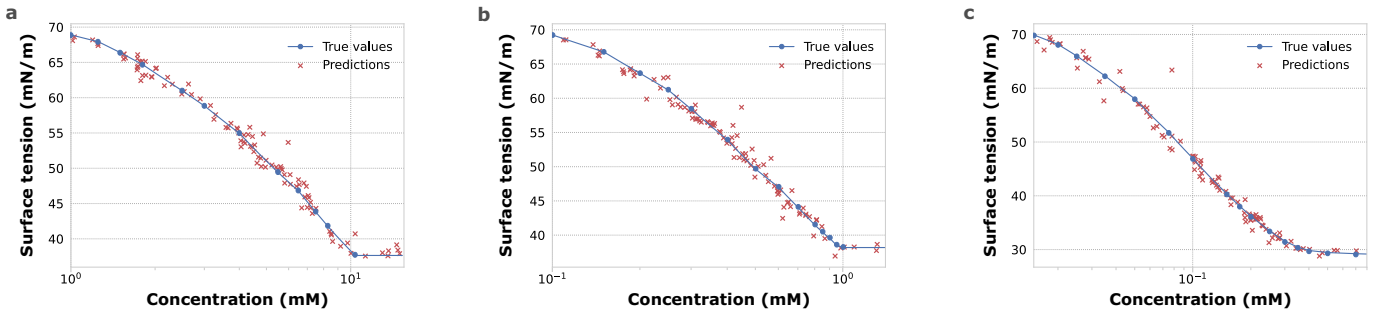

Fig. 5. Predictions from the test dataset on the adsorption isotherm of each surfactant used. With a solid blue line are indicated the pendant drop measurements and with red crosses the predictions from the machine learning algorithm. (a) Predictions on SDS. (b) Predictions on CTAB. (c) Predictions on Triton X-100.

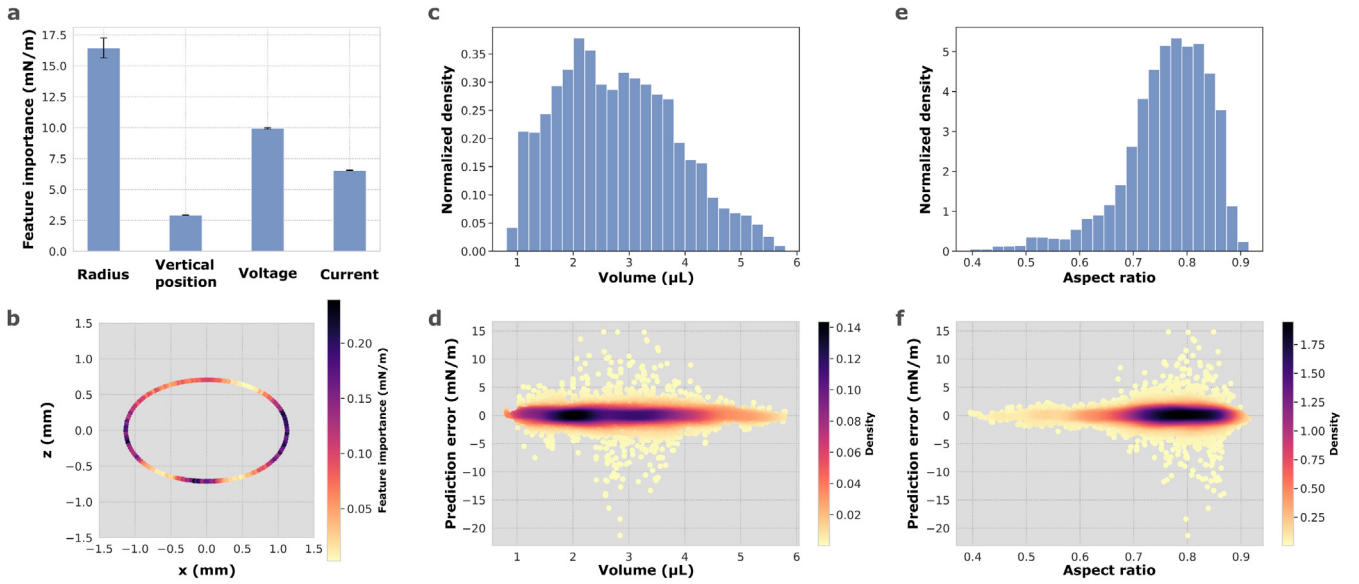

Fig. 6. (a) Bar plot that illustrates the importance of each feature that was used in the training of the neural network. (b) The 175 radii that define the droplet contour is color coded with respect to the feature importance. The darker the color, the higher the influence of that radius in the machine learning predictions. (c) Density distribution of volume in the test dataset. (d) Prediction error with respect to the volume. (e) Density distribution of aspect ratio in the test dataset. (f) Prediction error with respect to the aspect ratio of the droplet.

greatest contribution to the prediction, since they differentiate the most, depending on the characteristics of the droplet (*e.g.*, surface tension, volume, voltage *etc.*). Hence, they contain more useful information for establishing a correlation between the contour points, and the surface tension. The voltage, current, and position of the droplet are associated with the surface acoustic pressure on the droplet. Hence, there is a clear relation to the deformation of the droplet, with voltage having the greatest influence. Overall, it appears that the machine learning algorithm reaches a decision based on the physical parameters that we would expect to be the most relevant. The same feature importance analysis was performed with the in silico data, leading to the same conclusions (Fig. S9, Supporting Information).

To further investigate whether the source of prediction error is related to the size (*i.e.*, volume), or the deformation (*i.e.*, aspect ratio) of the droplet, we compared the density distributions of the volume (Fig. 6c), and aspect ratio (Fig. 6e) e) to the prediction error. In Fig. 6d, we observe that the error is relatively equally distributed throughout the volume range (Fig. 6c). A larger prediction error appears in the volume range of 2 to 4 μL, however, the majority of the contours lie in that range. As a result, the probability that a larger error may arise due to other parameters (*e.g.*, instabilities) increases. A similar tendency is observed between the aspect ratio range distribution (Fig. 6e) and the error distribution (Fig. 6f). A small fraction of higher error is observed in the range of 0.66 to 0.8, where the majority of the contours are found. Consequently, no conclusive correlation between the volume or aspect ratio value with the prediction error is identified. On the contrary, the machine learning algorithm appears to perform very well for larger volumes, and deformations.

4. Conclusions

Using a compact and highly stable acoustic levitator, the acquisition of a large experimental dataset suitable for a data-driven approach was possible. We developed a suitable machine learning algorithm that predicted the surface tension of acoustically levitated small-volume droplets of aqueous surfactant solutions. The neural network was first tested on in silico data without noise, and achieved a mean absolute error of 0.06 mN/m. When artificial noise was added, the error increased, however, the algorithm was still able to identify correlations between the input parameters and the surface tension. Once trained and tested on experimental data, the mean absolute error was 0.88 mN/m in a range of surface ten-

sion from 30 to 70 mN/m. In all cases, no overtraining occurred. An Open source framework containing the machine learning algorithms and the data is available on https://github.com/sargyri/Drop_Lev.

In regard to the rare previous attempts to correlate the surface tension with the shape deformation of acoustically levitated droplets [2–4,11,12], our approach is not restricted by the physical conditions that apply to the existing models. Specifically, the algorithm predicted equally well on experimental data with volume higher than 2.5 μL, and aspect ratios lower than 0.66, which offers higher flexibility and data availability for this type of contactless measurement. Furthermore, we were able to determine the surface tension by utilizing parameters that are easily accessible (*i.e.*, contour, voltage, current, position), and without the need of determining the surface acoustic pressure, often a source of large error. Finally, we achieved significantly better accuracy compared to previous work [2] that stated a 15% error in determining the shape of a droplet when the volume, acoustic pressure, and surface tension are known. We also achieved similar to better accuracy, as it was stated that for droplets with surface tension below 50 mN/m, the sensitivity of the technique was ± 2 mN/m [4].

One limitation of our study is the fact that only aqueous surfactant solutions with a density close to 1 g/ml were used. For measurements on other liquids, the acoustic impedance should actually be accounted for in the training of the neural network. As acoustic impedance is directly proportional to the density of liquids, this latter can be used as a proxy for it. However, due to the versatility of machine learning, it is expected that the neural network will perform equally well on liquids with various densities if trained with a more density-diverse dataset. The future work plans are to investigate this aspect along with the possibility of studying interfacial rheology in regimes that are difficult to attain with the pendant drop technique.

Data availability

Data will be made available on request.

Declaration of Competing Interest

The authors declare that they have no known competing financial interests or personal relationships that could have appeared to influence the work reported in this paper.

Acknowledgements

The authors are grateful for the financial support from the Swedish Research Council (VR) (Public, Sweden), and the Swedish Foundation for Strategic Research (SSF) (Non Profit, Sweden).

Appendix A. Supplementary material

Supplementary data associated with this article can be found, in the online version, at https://doi.org/10.1016/j.jcis.2023.02.077.

References

[1] D.P. Jackson, M.-H. Chang, Acoustic levitation and the acoustic radiation force, Am. J. Phys. 89 (4) (2021) 383–392, https://doi.org/10.1119/10.0002764.
[2] E.H. Trinh, C.-J. Hsu, Equilibrium shapes of acoustically levitated drops, J. Acoust. Soc. Am. 79 (5) (1986) 1335–1338, https://doi.org/10.1121/1.393660.
[3] Y. Tian, R.G. Holt, R.E. Apfel, Deformation and location of an acoustically levitated liquid drop, J. Acoust. Soc. Am. 93 (6) (1993) 3096–3104, https://doi.org/10.1121/1.415384.
[4] Y. Tian, R.G. Holt, R.E. Apfel, A new method for measuring liquid surface tension with acoustic levitation, Review of scientific instruments 66 (5) (1995) 3349–3354, https://doi.org/10.1063/1.1145506.
[5] R. Wüstneck, P. Enders, R. Miller, On the error propagation of experimental surface tension values to parameters of adsorption isotherms, Colloids Surf., A 100 (1995) 207–215, https://doi.org/10.1016/0927-7757(95)03164-9.
[6] M.A. Andrade, S. Polychronopoulos, G. Memoli, A. Marzo, Experimental investigation of the particle oscillation instability in a single-axis acoustic levitator, AIP Advances 9 (3) (2019) 035020, https://doi.org/10.1063/1.5078948.
[7] A. Marzo, A. Barnes, B.W. Drinkwater, Tinylev: A multi-emitter single-axis acoustic levitator, Rev. Sci. Instrum. 88 (8) (2017) 085105, https://doi.org/10.1063/1.4989995.
[8] J.D. Berry, M.J. Neeson, R.R. Dagastine, D.Y. Chan, R.F. Tabor, Measurement of surface and interfacial tension using pendant drop tensiometry, Journal of colloid and interface science 454 (2015) 226–237.
[9] levitate, https://github.com/AppliedAcousticsChalmers/levitate (2021).
[10] C. Andersson, J. Ahrens, Minimum trap separation for acoustical levitation using phased ultrasonic transducer arrays, Universitätsbibliothek der RWTH Aachen, 2019.
[11] P.L. Marston, Shape oscillation and static deformation of drops and bubbles driven by modulated radiation stresses—theory, J. Acoust. Soc. Am. 67 (1) (1980) 15–26, https://doi.org/10.1121/1.383798.
[12] P.L. Marston, S.E. LoPorto-Arione, G.L. Pullen, Quadrupole projection of the radiation pressure on a compressible sphere, J. Acoust. Soc. Am. 69 (5) (1981) 1499–1501, https://doi.org/10.1121/1.385785.
[13] J. Canny, A computational approach to edge detection, IEEE Transactions on pattern analysis and machine intelligence PAMI-8 6 (1986) 679–698.
[14] Structural analysis and shape descriptors, https://docs.opencv.org/4.x/d3/dc0/group__imgproc__shape.html#gadf1ad6a0b82947fa1fe3c3d497f260e0 (2022).
[15] A. Fisher, C. Rudin, F. Dominici, All models are wrong, but many are useful: Learning a variable's importance by studying an entire class of prediction models simultaneously, J. Mach. Learn. Res. 20 (177) (2019) 1–81.
[16] Interpretable machine learning, https://github.com/christophM/interpretable-ml-book (2020).